

Article

Curcumin and Graphene Oxide Incorporated into Alginate Hydrogels as Versatile Devices for the Local Treatment of Squamous Cell Carcinoma

Lorenzo Francesco Madeo^{1,*}, Patrizia Sarogni², Giuseppe Cirillo^{3,*}, Orazio Vittorio^{4,5,6}, Valerio Voliani², Manuela Curcio³, Tyler Shai-Hee^{4,5,6}, Bernd Büchner^{1,7}, Michael Mertig^{8,9} and Silke Hampel¹

- ¹ Leibniz Institute of Solid State and Material Research Dresden, 01069 Dresden, Germany; b.buechner@ifw-dresden.de (B.B.); s.hampel@ifw-dresden.de (S.H.)
- ² Center for Nanotechnology Innovation, Istituto Italiano di Tecnologia, Piazza San Silvestro 12, 56127 Pisa, Italy; patrizia.sarogni@iit.it (P.S.); valerio.voliani@iit.it (V.V.)
- ³ Department of Pharmacy Health and Nutritional Science, University of Calabria, 87036 Rende, Italy; manuela.curcio@unical.it
- ⁴ Children's Cancer Institute, Lowy Cancer Research Centre, University of New South Wales, High Street, Randwick, NSW 2052, Australia; ovittorio@ccia.org.au (O.V.); tshai-hee@ccia.org.au (T.S.-H.)
- ⁵ School of Women's and Children's Health, University of New South Wales, Kensington, NSW 2052, Australia
- ⁶ ARC Centre of Excellence in Convergent Bio-Nano Science and Technology, Australian Centre for NanoMedicine, University of New South Wales, Kensington, NSW 2052, Australia
- ⁷ Institute of Solid State and Materials Physics, Technische Universität Dresden, 01062 Dresden, Germany
- ⁸ Institute of Physical Chemistry, Technische Universität Dresden, 01062 Dresden, Germany; michael.mertig@tu-dresden.de
- ⁹ Kurt-Schwabe-Institut für Mess- und Sensortechnik Meinsberg e.V., 04736 Waldheim, Germany
- * Correspondence: l.f.madeo@ifw-dresden.de (L.F.M.); giuseppe.cirillo@unical.it (G.C.); Tel.: +49-35-1465-9883 (L.F.M.); +39-09-8449-3208 (G.C.)



Citation: Madeo, L.F.; Sarogni, P.; Cirillo, G.; Vittorio, O.; Voliani, V.; Curcio, M.; Shai-Hee, T.; Büchner, B.; Mertig, M.; Hampel, S. Curcumin and Graphene Oxide Incorporated into Alginate Hydrogels as Versatile Devices for the Local Treatment of Squamous Cell Carcinoma. *Materials* **2022**, *15*, 1648. <https://doi.org/10.3390/ma15051648>

Academic Editor: Marilena Vlachou

Received: 7 February 2022

Accepted: 18 February 2022

Published: 22 February 2022

Publisher's Note: MDPI stays neutral with regard to jurisdictional claims in published maps and institutional affiliations.



Copyright: © 2022 by the authors. Licensee MDPI, Basel, Switzerland. This article is an open access article distributed under the terms and conditions of the Creative Commons Attribution (CC BY) license (<https://creativecommons.org/licenses/by/4.0/>).

Abstract: With the aim of preparing hybrid hydrogels suitable for use as patches for the local treatment of squamous cell carcinoma (SCC)-affected areas, curcumin (CUR) was loaded onto graphene oxide (GO) nanosheets, which were then blended into an alginate hydrogel that was crosslinked by means of calcium ions. The homogeneous incorporation of GO within the polymer network, which was confirmed through morphological investigations, improved the stability of the hybrid system compared to blank hydrogels. The weight loss in the 100–170 °C temperature range was reduced from 30% to 20%, and the degradation of alginate chains shifted to higher temperatures. Moreover, GO enhanced the stability in water media by counteracting the de-crosslinking process of the polymer network. Cell viability assays showed that the loading of CUR (2.5% and 5% by weight) was able to reduce the intrinsic toxicity of GO towards healthy cells, while higher amounts were ineffective due to the antioxidant/prooxidant paradox. Interestingly, the CUR-loaded systems were found to possess a strong cytotoxic effect in SCC cancer cells, and the sustained CUR release (~50% after 96 h) allowed long-term anticancer efficiency to be hypothesized.

Keywords: curcumin; graphene oxide; alginate hydrogels; hybrid hydrogels; ionic crosslinking; squamous cell carcinoma

1. Introduction

The interest in graphene and the materials derived from it for biomedical applications has grown tremendously in recent years [1–4]. In particular, graphene oxide (GO) has been largely investigated as a promising therapeutic delivery vehicle because of its particular properties [5,6]. Aside from the high surface-area-to-volume ratio and the sp² carbon layer that allows π - π interactions with hydrophobic molecules [7,8], its oxygen-rich functionalities can form hydrogen bonds and electrostatic interactions with hydrophilic molecules [9,10], providing new opportunities to effectively bind to almost any type of

organic molecule [11,12]. Such functional flexibility makes GO a useful platform that is capable of controlling the release of a wide range of therapeutic molecules, including chemotherapeutics, peptides, genes, and naturally occurring compounds [13–17].

Among the plethora of naturally occurring molecules used in biomedicine, our interest was drawn to curcumin (CUR), a diferuloylmethane constituent of the yellow pigments isolated from *Curcuma longa*, which is well known for its antioxidant, radical-scavenging, antimicrobial, and anti-inflammatory properties [18,19]. It has also shown potent anti-proliferative effects against several cancers due to its ability to interfere with different cellular pathways involved in carcinogenesis [20,21]. Therefore, CUR has been tested both in vitro and in vivo against a large number of tumors [22–24], thus sparking its interest as a potential skin cancer treatment [25,26], whereby several studies have supported CUR as a potential candidate for the treatment of squamous cell carcinoma (SCC) [27–29].

SCC is an invasive and lethal epithelial malignancy representing approximately 20% to 25% of non-melanoma skin cancers [30]. It arises from the prickle–squamous cell layers of the epidermis, shows keratinocytic differentiation [31], and is capable of metastasis to regional lymph nodes.

Although local excision of smaller cutaneous SCC is frequently performed with acceptable outcomes, the treatment of patients with multiple lesions or condemned skin, particularly in the head and neck, is a more difficult challenge [30,32,33]. Therefore, the use of bioactive agents to treat such conditions might be a promising solution through both systemic and local administration [34–36].

Although an enormous number of studies have enlightened readers about the outcomes of CUR on a molecular level, its use as an effective pharmaceutical lead has been challenging, with no satisfying results up until now due to its poor solubility, low bioavailability, and uncontrolled reactivity in vivo [37,38]. For these reasons, a proper topical administration of CUR on a skin area affected by SCC might be desirable.

Providing an appropriate vehicle system for the controlled release of CUR in such applications is crucial, since high topical dosages may result in toxicity concerns [39]. Among the different delivery systems exploited in the literature, the peculiar features of GO can lead to the development of highly effective dosage forms with prolonged release [40].

In order to achieve an acceptable degree of stability and hydrophilicity, hybrid GO–hydrogel systems were proposed, which allow the combination of the favorable properties of both counterparts: the high hydrophilicity and biocompatibility of hydrogel systems and the high drug affinity of GO [41,42]. Among the polymeric materials adopted to enhance the stability of graphene-based carriers, alginate showed several interesting features [43].

Alginate is a natural polysaccharide found in brown algae; it is biocompatible, non-toxic, non-thrombogenic, and non-immunogenic, and it is approved by the Food and Drug Administration (FDA) for various medical applications [44,45]. Its capacity to form a stable and swelling hydrogel in the presence of divalent cations (e.g., calcium ions) through ionotropic gelation has made this polymer of great interest for multiple medical applications, including the fabrication of scaffolds for tissue regeneration, wound healing, and protein/drug delivery systems [46,47].

In this study, CUR-loaded GO sheets were blended into alginate polymer and crosslinked by means of calcium ions, resulting in a flexible and mechanically stable hybrid hydrogel film. Such drug delivery systems have been proposed as patches for external use and are capable of performing an effective and sustained release of CUR onto SCC-affected areas.

2. Materials and Methods

2.1. Synthesis of Hybrid Hydrogels

Graphene oxide (GO) powder was added to a 2.0% (*w/v*) sodium alginate (ALG) solution in double-distilled water (ddH₂O) with a GO-to-ALG ratio of 2.0% by weight. The mixture was thoroughly stirred for 15 min and then sonicated using a horn-tipped ultrasonic probe with 20% amplitude (BANDELIN electronic GmbH, Berlin, Germany)

for 15 min in order to crack the GO aggregates and obtain a fine dispersion. Thereafter, a selected amount of a 0.5% (*w/v*) solution of curcumin (CUR) in ethanol was added to obtain CUR-to-ALG ratios of 2.5, 5.0, and 7.5% (*w/w*) across separate experiments.

To obtain a platform for the physical crosslinking of the hybrid dispersion, a solution consisting of 1.0% *w/v* agar and 0.2 M calcium chloride (0.2 M) in ddH₂O was heated up until boiling and left to cool in a Petri dish. The solution containing ALG, GO, and CUR was then gently poured and left to crosslink at 40 °C for 2 h. The obtained CUR@H_{ALG}-GO hydrogel was peeled off the agar gel below and washed in ddH₂O to remove unreacted species. Afterwards, the hydrogel was dried at 40 °C for 12 h. The same approach without the insertion of CUR (H_{ALG}-GO and H_{ALG}) or GO (H_{ALG} and CUR@H_{ALG}) in the reaction feed was used to prepare the control samples.

All chemicals were purchased from Merck/Sigma Aldrich, Darmstadt, Germany.

2.2. Instruments

Attenuated total reflectance Fourier transform infrared spectroscopy (ATR-FTIR) spectra were recorded on an IFS/66v/S (BRUKER Optic GmbH, Karlsruhe, Germany).

Dynamic light scattering (DLS) analyses were performed with a 90 Plus Particle Size Analyzer (Brookhaven Instruments Corp, Holtsville, NY, USA) at 25.0 ± 0.1 °C with a laser operating at 658 nm while measuring the autocorrelation function at 90°.

Thermogravimetric analysis (TGA) was performed on an SDT Q600 (TA Instruments, Hüllhorst, Germany) under a nitrogen atmosphere with the following conditions: 10 mg initial sample weight, 10 mL min⁻¹ N₂ flow, 25–800 °C temperature range, and 10 °C min⁻¹ heating rate.

Optical microscope images were taken with an Axio Imager.A2m (Zeiss, Oberkochen Germany).

Scanning electron microscope (SEM) images of samples were taken with a NOVA NanoSEM 200 [0–30 kV] (Thermo Fisher Scientific, Hillsboro, OR, USA) by depositing samples onto self-adhesive conductive carbon tape (Plano GmbH, Wetzlar, Germany).

Atomic force microscopy (AFM) images were taken with a Dimension Icon (Bruker) operating in the tapping mode, and they were examined with the Nanoscope Analysis software, version 1.8.

2.3. Evaluation of Water Affinity

The water affinity of the blank and hybrid hydrogels was evaluated by immersing weighted specimens of each sample (~5.0 cm²) in the swelling medium, which consisted of phosphate-buffered saline (PBS) solution (10⁻⁴ M, pH 7.4), at 37 °C. At predetermined time intervals, surface moisture was removed by blotting samples with a tissue, and the samples were weighed. The water affinity was expressed as the water content percentage (WR) according to Equation (1):

$$WR = \frac{W_s - W_d}{W_d} \times 100 \quad (1)$$

Here, W_d and W_s represent the weights of samples in the dried and swollen states, respectively.

All chemicals were purchased from Merck/Sigma Aldrich, Darmstadt, Germany.

2.4. CUR Release Profiles

In vitro CUR release profiles were determined with the dissolution method. In separate experiments, weighted specimens of ~1 cm² of loaded hydrogels were immersed in 10 mL of releasing medium consisting of a PBS (0.001 M, pH 7.4)/ethanol mixture (6/4, *v/v*) and maintained at 37.0 ± 0.1 °C in a water bath with alternate shaking. At predetermined time intervals, 1.0 mL of release medium was withdrawn, filtered with Iso-Disc™ Filters PTFE 25–4 (25 mm × 0.45 μm, Merck/Sigma Aldrich, Darmstadt, Germany), and, to ensure sink conditions throughout the experiment, replaced with fresh release medium. The amount of CUR in the solution was determined by UV–Vis analysis on an Evolution

201 spectrophotometer (ThermoFisher Scientific, Hillsboro, OR, USA) operating with 1.0 cm quartz cells set at 430 nm using the calibration curve of CUR. The amount of CUR released was expressed according to Equation (2):

$$\text{CUR release} = \frac{M_t}{M_0} \quad (2)$$

where M_t and M_0 are the CUR amounts (mg) detected at time t and loaded into the hydrogels, respectively.

All chemicals were purchased from Merck/Sigma Aldrich, Darmstadt, Germany.

2.5. Cell Culture

Human bronchial epithelial cells (HBEpc) and human squamous cell carcinoma SCC-25 (HPV-negative) were purchased from the American Type Culture Collection (ATCC, Manassas, VA, USA). HBEpc were cultured in ready-to-use bronchia/trachea epithelial cell growth medium (Cell Applications) supplemented with 10% fetal bovine serum (FBS), while the SCC-25 cells were grown in a complete medium composed of a 1:1 mixture of Dulbecco's modified Eagle's medium and Ham's F12 (Invitrogen) supplemented with 10% FBS, 4 mM L-glutamine, 1 mM sodium pyruvate, 100 U/mL penicillin–100 mg/mL streptomycin, and 400 ng/mL of hydrocortisone. Cells were maintained at 37 °C in a humidified incubator with 5% CO₂ atmosphere.

2.6. Cytotoxic Assays

The cytotoxicity of the unloaded H_{ALG} and H_{ALG-GO} or the CUR-loaded CUR@H_{ALG} and CUR@H_{ALG-GO} was evaluated through microscopic observation and cell counting using the trypan blue method in a time-course experiment [48]. A small piece of hydrogel film of approximately 1.0 cm² was placed inside a 35 mm tissue culture dish and hydrated overnight with the supplemented culture medium. The following day, the HBEpc and SCC-25 cells were trypsinized and counted, and 2 × 10⁵ cells were seeded (0 h). The cytotoxic effects were evaluated after 24 and 48 h of exposure with the hydrogel film.

3. Results and Discussion

3.1. Synthesis of the Hybrid Hydrogel and CUR Loading

Alginate hydrogels that were obtained via either chemical or physical crosslinking methods have been extensively explored as a platform for sustained release of drugs due to their capability of entrapping a wide range of bioactive molecules [43]. The achievement of physical crosslinking presents a significant advantage over chemical crosslinking strategies, since the latter often require the use of crosslinking agents, solvents, and other chemicals, which need to be removed at the end of the process [49,50].

In our experimental conditions, since a stable and homogenous dispersion of GO into the hybrid film was needed to ensure the formation of the hybrid GO system [51], a straightforward approach that did not involve the use of any toxic chemical species was adopted. In detail, a GO-to-ALG ratio of 2.0% (by weight) was chosen, since lower GO amounts could lead to the formation of less effective dosage forms, while higher ratios could result in an unstable dispersion in which large GO aggregates would be formed. This statement was confirmed by dynamic light scattering (DLS) measurements: the hydrodynamic diameter of GO@ALG (2%) in the reaction feed was found to be 287 nm, becoming 785 nm when a higher amount of GO (2.5%) was used.

Then, to promote the interaction of GO and CUR, a solution of CUR in ethanol (5 mg mL⁻¹) was added while taking the need to use a lower amount of ethanol, which could otherwise cause alginate precipitation, into consideration. The crosslinking step was performed with the aid of an agar gel platform for calcium ion diffusion. With this method, the calcium ions slowly diffused into the polymeric blend [52], resulting in a homogenous and effective ionotropic gelation with the formation of CUR@H_{ALG-GO}, as sketched in Figure 1. Control samples were prepared by using the same approach without the insertion

of CUR (H_{ALG-GO} and H_{ALG}) or GO (H_{ALG} and $CUR@H_{ALG}$) into the reaction feed before the crosslinking step.

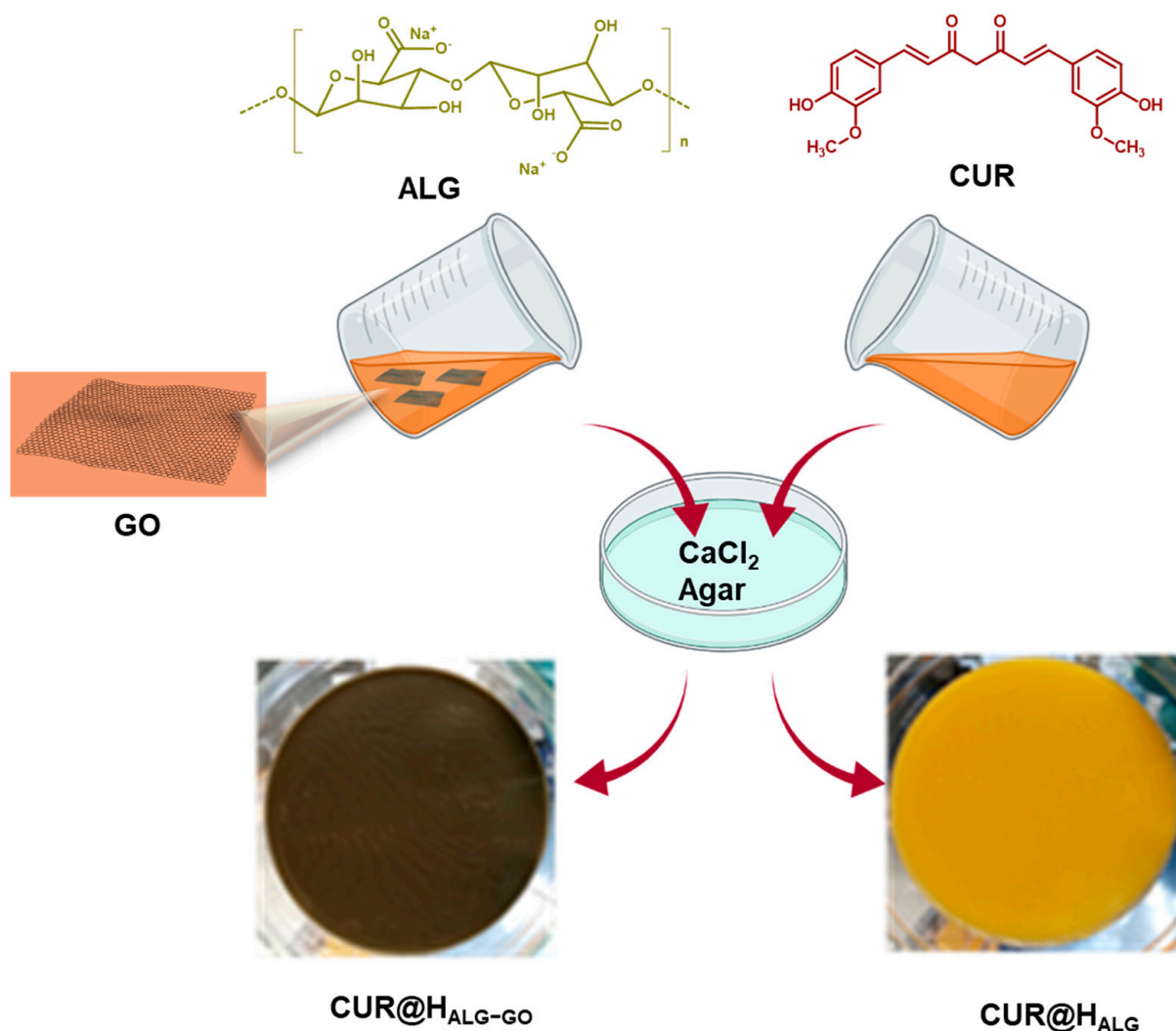


Figure 1. Schematic representation of CUR@H_{ALG}-GO synthesis.

3.2. Characterization Procedure

Hybrid hydrogels were characterized with a multi-technique approach, allowing for the determination of different properties, including the morphological, chemical, and thermal properties, as well as the water affinity.

The investigation of CUR@H_{ALG}-GO with both optical and electron microscopy allowed for the effective incorporation of CUR and GO to be visualized (Figure 2). Moreover, homogeneous incorporation of GO into the polymer network was clearly evident by comparing the SEM images of the blank and hybrid systems (Figure 2b). The H_{ALG} sample showed a smooth surface, while the GO within H_{ALG}-GO appeared as embedded dots emerging from the hydrogel surface, as confirmed by the AFM images (Figure 2c).

The attenuated total reflectance Fourier transform infrared spectroscopy (ATR-FTIR) patterns of CUR@H_{ALG}-GO showed the presence of the typical absorption peaks of all components of the hybrid systems (Figure 3).

The ALG showed bands at 3000–3600 cm⁻¹ (stretching of OH bonds) and 1600–1422 cm⁻¹ (asymmetric and symmetric stretching of carboxyl groups) [53]. The same groups were found in GO, with the stretching of OH and COOH located at 3399 and 1753 cm⁻¹ [54], respectively, whilst the peak at 1074 cm⁻¹ was attributed to the stretching of the C-O

group. In the CUR spectrum, the signals at $3300\text{--}3550\text{ cm}^{-1}$ were assigned to the stretching vibrations of phenolic groups, with signals at 1466 and 1258 cm^{-1} corresponding to the stretching of aromatic $\text{C}=\text{C}$ and bending of phenolic $\text{C}-\text{O}$, respectively [55].

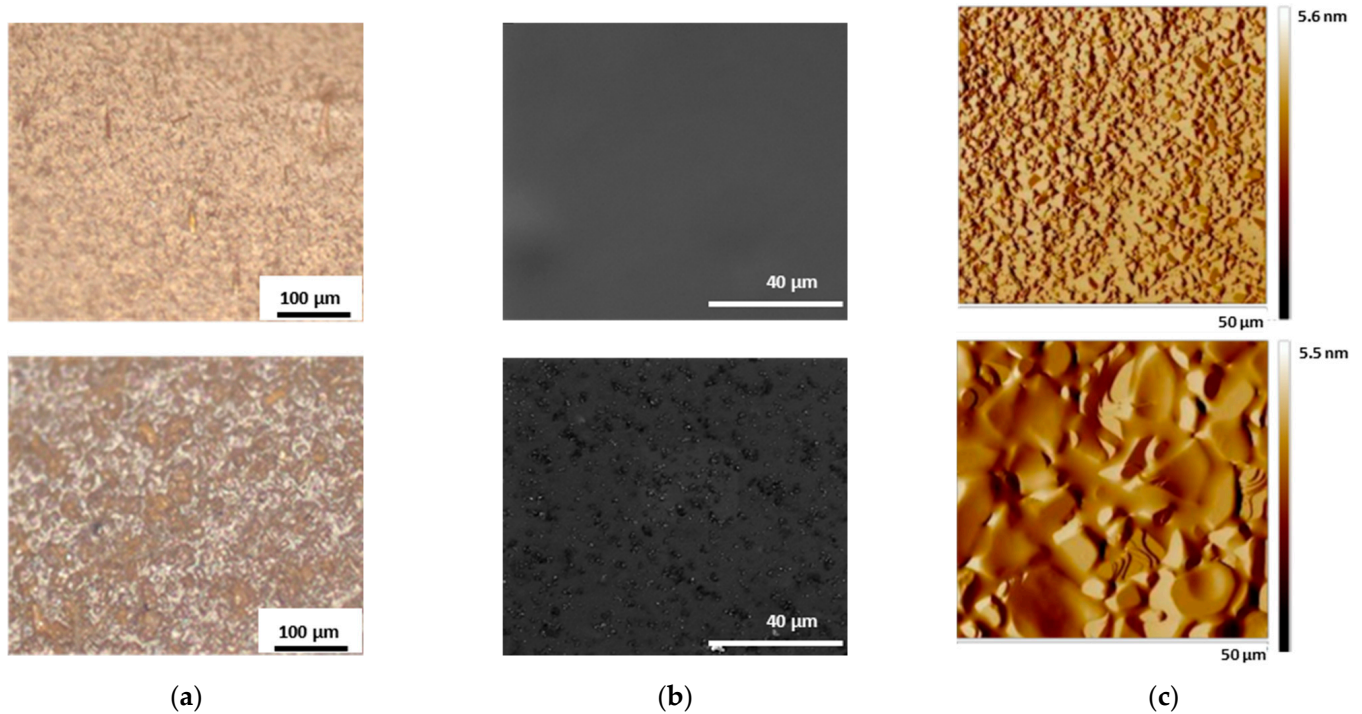


Figure 2. (a) Optical, (b) SEM, and (c) AFM images of CUR@HALG (top) and CUR@HALG-GO (bottom) showing: (a) the typical orange color of CUR loaded into the polymer networks; (b) the homogeneous incorporation of GO into the hybrid materials; (c) the presence of the GO sheet emerging from the hydrogel surface.

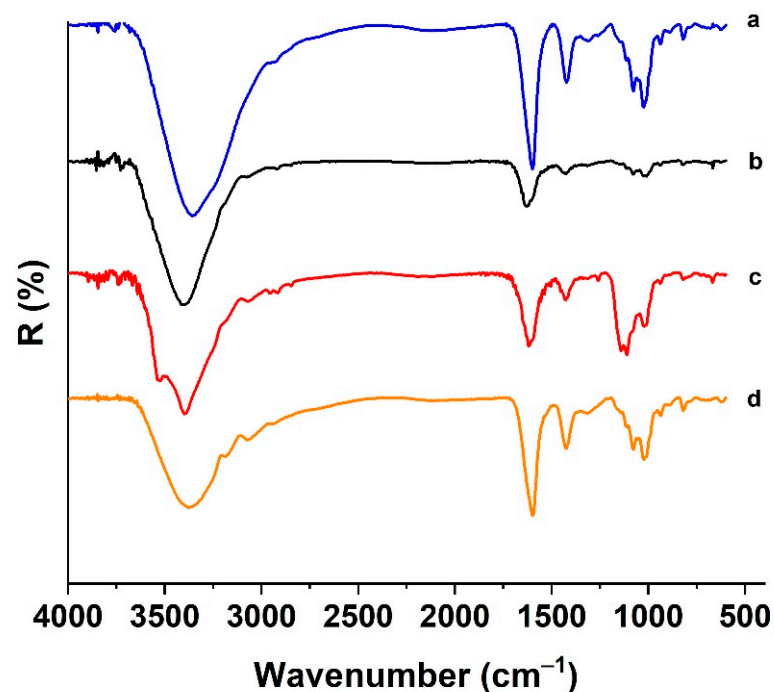


Figure 3. ATR-FTIR spectra of (a) ALG, (b) GO, (c) CUR, and (d) CUR@HALG-GO.

A thermogravimetric analysis (TGA) of the CUR, CA-GO, CA-CUR, and CA-GO-CUR hydrogels was performed in order to determine their thermal stability (Figure 4a).

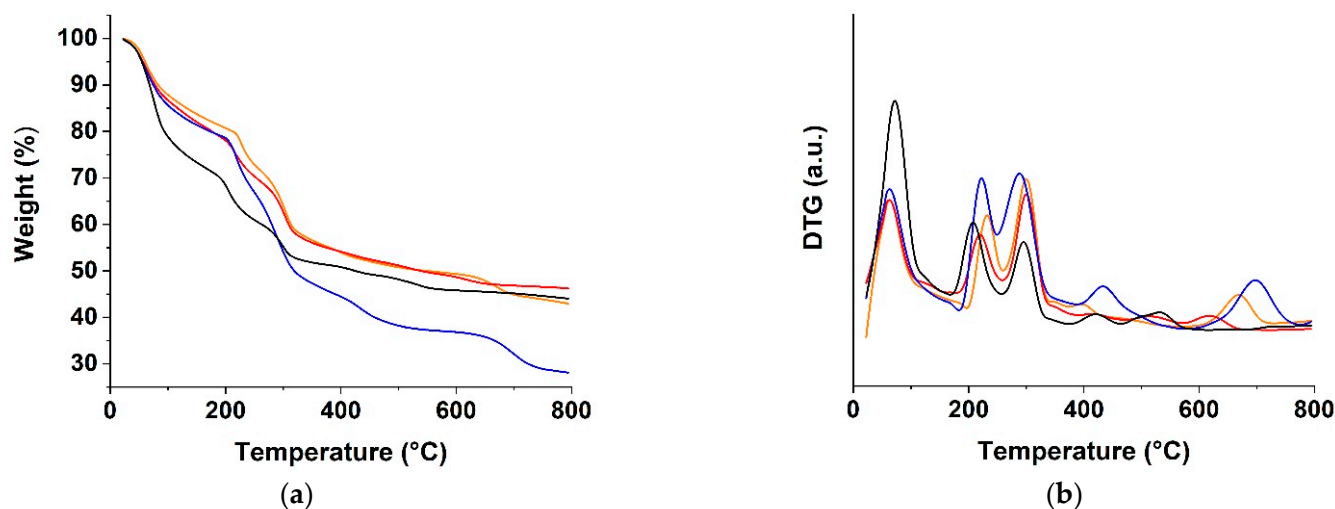


Figure 4. (a) TGA and (b) DTG curves of H_{ALG} (blue lines), H_{ALG-GO} (black lines), $CUR@H_{ALG}$ (red lines), and $CUR@H_{ALG-GO}$ (orange lines).

All of the curves showed a first weight loss at around 100 °C, which mainly correlated with the elimination of the free water. H_{ALG-GO} was characterized by the highest content of free water, with a weight loss of up to 30% in the 100–170 °C temperature range, a value that was reduced by 20% in the case of H_{ALG} . The effect of the incorporation of GO into the polymer network was the result of the balance between the hydrophobic character of the GO sheets due to the sp^2 carbon layer and the presence of oxygen-rich functionalities on the edge [56]. Here, the increased specific surface area of the hybrid hydrogels due to the incorporation of the polar surface of GO was responsible for the increased weight loss in the first temperature range. Further incorporation of highly hydrophobic CUR molecules into the $CUR@H_{ALG-GO}$ sample was found to counter this effect.

Moving to higher temperatures (200–300 °C), two degradation peaks related to the decomposition of free alginate chains could be observed, with the analysis of the derivative thermogravimetric (DTG) curve showing that the second peak was shifted to higher temperatures in the GO-containing samples (Figure 4b) due to the increased chain immobilization, resulting in a higher thermal stability.

Above 300 °C, the fracture of glycosidic bonds and the decarbonylation of alginate chains led to the release of CO_2 in addition to other small molecules and the consequent weight loss in the case of H_{ALG} [57]. These events were hindered in the other hydrogel samples as a consequence of the enhanced stabilization of the polymer structure by the presence of both CUR and GO. CUR and GO, indeed, were able to greatly affect the chain mobility and crosslinking density of the polymer networks.

Then, swelling studies were performed in PBS at pH 7.4 to evaluate the water uptake and stability of the samples in a solution with an ion concentration comparable to that found in the human body (Figure 5).

Due to the combination of two different effects, H_{ALG-GO} showed a reduced degree of swelling compared to H_{ALG} . On one hand, it is well known that the swelling capacity of any kind of hydrogel sample decreases with an increase in the crosslinking degree, suggesting that the presence of GO inside the polymer network tightened the alginate chains, thus acting as a bridge. On the other hand, the hydrophobic effect of the C-C layer on the GO surface overcame the hydrophilicity conferred by the oxygen-rich groups when the exposure to water was longer than 2 h.

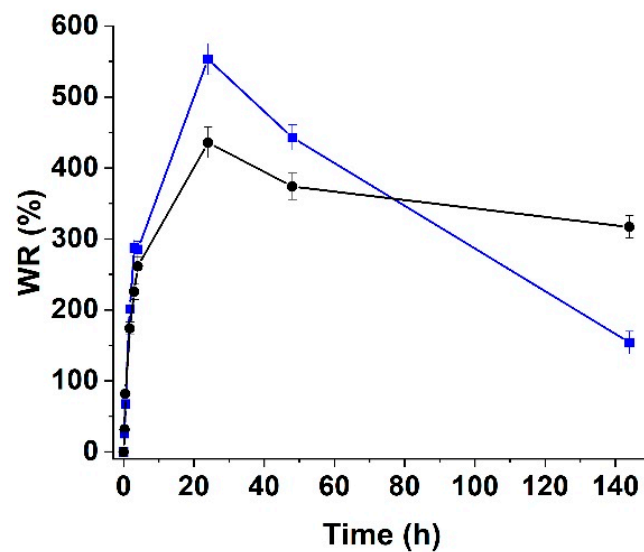


Figure 5. Swelling profiles of H_{ALG} (blue line) and H_{ALG-GO} (black line) at pH 7.4.

Further extending the reaction time (>24 h) resulted in the destabilization of ALG networks due to the interference between calcium and sodium ions, thus resulting in the disruption of crosslinking and partial dissolution of alginate into the water solution with a reduction in the swelling degree [58]. Due to the incorporation of GO, the chain stabilization was found to counteract this event, thus resulting in a less pronounced reduction in the swelling properties.

3.3. Characterization of Biological Impact

To evaluate the efficiency of hybrid hydrogels as a delivery vehicle, three different CUR-to-hydrogel ratios (by weight) were used to incorporate the bioactive molecule, namely, 2.5, 5.0, and 7.5%. Then, the toxicity profile was investigated in normal human bronchial epithelial cells (HBEpC) in terms of cell viability after 24 and 48 h of incubation (Figure 6).

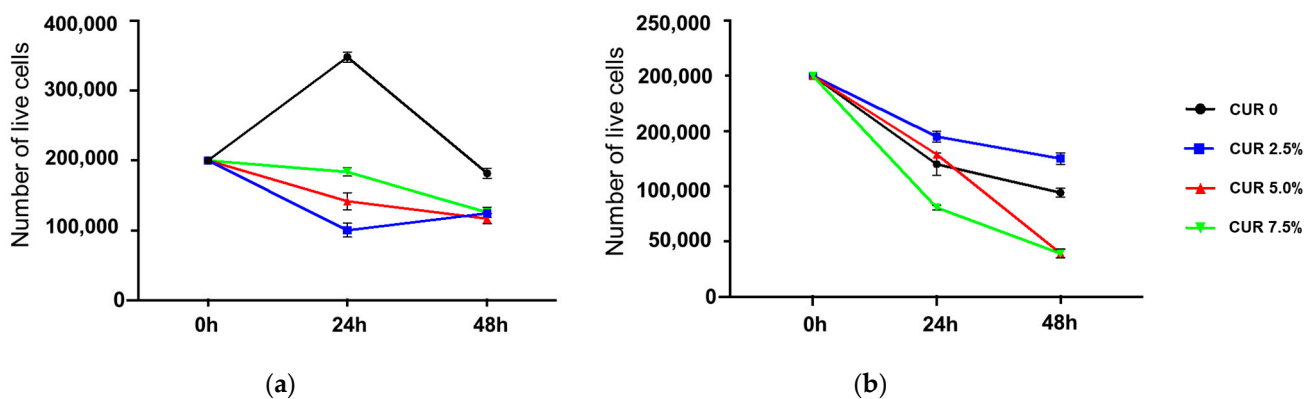


Figure 6. Cell viability profile of HBEpC 24 and 48 h after incubation with CUR-loaded (a) H_{ALG} and (b) H_{ALG-GO}. Data are expressed as means \pm SD of three counts.

The analysis of the results clearly proved that the unloaded blank and hybrid hydrogels possessed completely different behaviors. H_{ALG} (Figure 6a) was found to be non-toxic and was well tolerated by HBEpC, with the number of living cells not being significantly reduced even after 48 h of incubation. Moreover, they could act to support cell growth and proliferation [59,60].

On the contrary, time-dependent toxicity was recorded in the case of H_{ALG-GO} (Figure 6b), with the viability (%) decreasing down to 50% after 48 h of incubation. These results may be related to both chemical and biological reasons. At first, the adopted synthetic strategy

should be taken into consideration to explain the differences between the obtained results and the available data from the literature, which claim the complete non-toxicity of hybrid alginate- and graphene-oxide-based systems, including those of our research group [61]. In this study, the GO-to-hydrogel ratio (2%) was significantly higher than those previously employed (1.15%); thus, cells were exposed to different amounts of GO, and the crosslinking step consisted of a simple ionic gelation without the need for other reactants (such as the highly biocompatible acrylate monomers that were previously employed), which could also act as an obstacle to the direct interactions of the hydrogel and cell membrane.

In our conditions, even after 24 h of incubation with H_{ALG-GO}, the cells started to lose their shape, suggesting the induction of cell death, with the effect being more evident after longer incubation times (Figure 7).

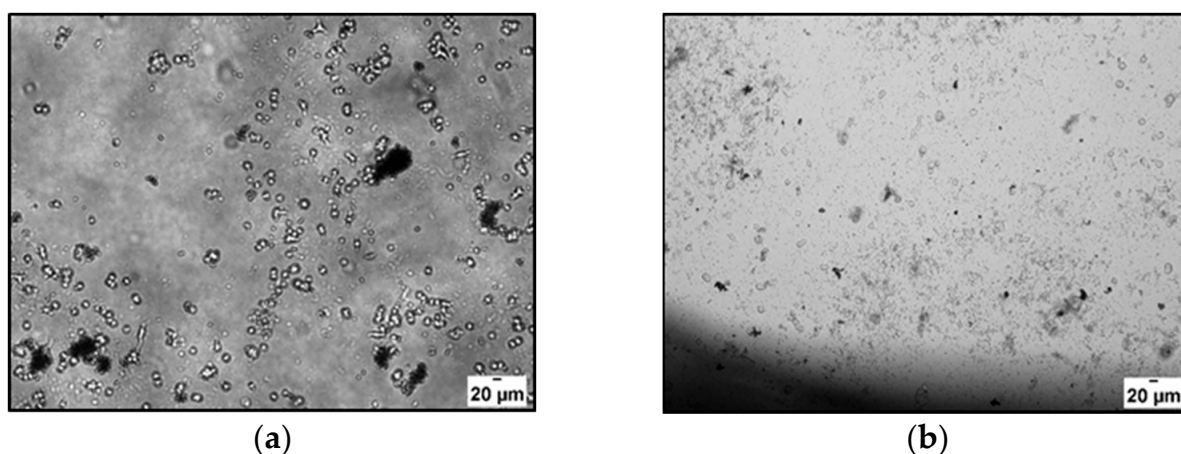


Figure 7. Optical microscope images of HBEpC after (a) 24 and (b) 48 h of incubation with H_{ALG-GO}.

When considering the biological effects arising from the hydrogel–cell interactions, it should be pointed out that although it is considered highly biocompatible, it has been reported that GO can show cytotoxic effects due to its interference with the cell redox state, mainly in the extracellular media [62]. This is only partly related to the structure of GO, which consists of a π – π surface layer with oxygen-rich functionalities and can exert either pro- or antioxidant properties depending on the environmental conditions [63]. The main determining phenomenon at the basis of GO's cytotoxicity is due to its adsorption properties: GO can indeed adsorb nutrients from the extracellular compartment, thus inducing nutrient depletion and oxidative stress at relatively high GO concentrations [64]. Moreover, it was reported that GO is able to induce the production of reactive oxygen species (ROS) in cell culture media, which is a further confirmation of the extracellular nature of GO's toxicity [65].

In our condition, the oxidative nature of cell toxicity was confirmed when considering the effect of CUR-loaded samples, with the effect on cell viability being a function of both CUR concentration and incubation time. CUR@H_{ALG-GO} 2.5% (Figure 6b, blue lines) was found to be less toxic than H_{ALG-GO} after 24 and 48 h of incubation. When considering CUR@H_{ALG-GO} 5.0% (Figure 6b, red lines), the protective effect was recorded only after 24 h, while an increase in toxicity was recorded with longer incubation times. The antioxidant/prooxidant paradox can help understand this phenomenon, since it is well known that higher concentrations of antioxidant species in an active redox environment can lead to an increase in oxidative stress, rather than a decrease [66,67]. The same hypothesis can be used to explain the increased cell toxicity of CUR-loaded H_{ALG} samples at all tested CUR concentrations.

Next, we investigated the viability of cancerous SCC-25 cells upon incubation with unloaded and loaded hydrogels (Figure 8).

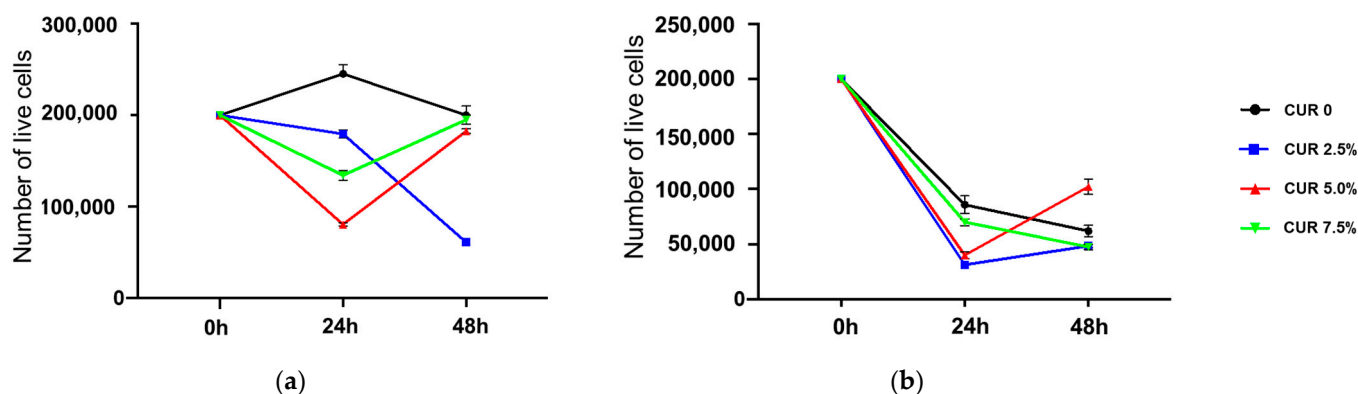


Figure 8. Cell viability profile of SCC-25 cells after 24 and 48 h of incubation with CUR-loaded (a) CUR@HALG and (b) CUR@HALG-GO. Data are expressed as means \pm SD of three counts.

The effects of unloaded the HALG and HALG-GO samples (Figure 8, black lines) were similar to those recorded for the HBEpC, with a higher toxicity recorded for HALG-GO. More interesting results were obtained when the CUR-loaded samples (2.5%) were used. Here, the polyphenol was found to counteract cell death upon loading on HALG, while the cytotoxicity was retained and even enhanced when HALG-GO was used as a delivery device (Figure 9). It is evident, indeed, that either the cell number or morphology was altered with increased CUR concentrations, suggesting the induction of cell death.

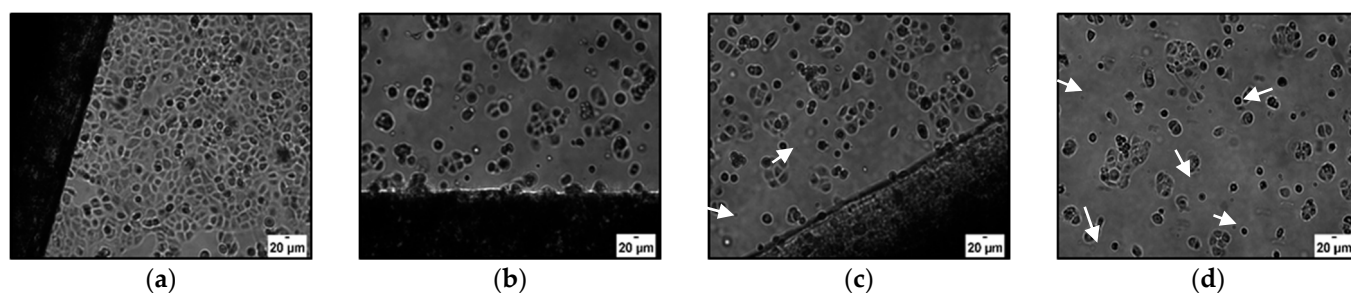


Figure 9. Microscope images of SCC-25 cells 24 h after incubation with (a) HALG-GO, (b) CUR@HALG-GO 2.5%, (c) CUR@HALG-GO 5.0%, and (d) CUR@HALG-GO 7.5%. Arrows indicate apoptotic cells.

To explain this behavior, it should be considered that, like many other polyphenols, CUR was proved to be highly toxic for cancer cells while being tolerated by healthy cells due to the different cell redox states [68]. Thus, the final effects of CUR-loaded hydrogels were the result of the alteration of the cells' redox state at either the extracellular or intracellular level, resulting in pronounced anticancer activity and reduced toxicity in healthy cells.

These results are very promising for future applications, although further experiments are required to properly understand the biological pathways involved and to design more effective systems to be applied in in vivo experiments.

3.4. CUR Release Experiments

To better understand the results of the biological impact of the synthesized hydrogels and to evaluate the possibility of guaranteeing a controlled CUR release over time, we extensively investigated the CUR release profiles of the HALG and HALG-GO samples. Samples loaded with the highest ratios of CUR (5.0 and 7.5%) were found to possess a significantly high burst release in the first experimental times, reaching M_t/M_0 values of 0.9 (HALG) and 0.7 (HALG-GO) after 2.0 h; thus, they were not investigated in this characterization.

The release profiles of the 2.5% CUR-loaded samples are depicted in Figure 10.

As expected, the highest affinity of GO for CUR, resulting in π - π stacking interactions between the aromatic rings of the polyphenols and the sp^2 carbon layer of the carbon

nanostructure, led to a more sustained release in the case of the hybrid H_{ALG-GO} sample, with M_t/M_0 values that did not reach 50% even after 96 h (>70% in the case of H_{ALG}).

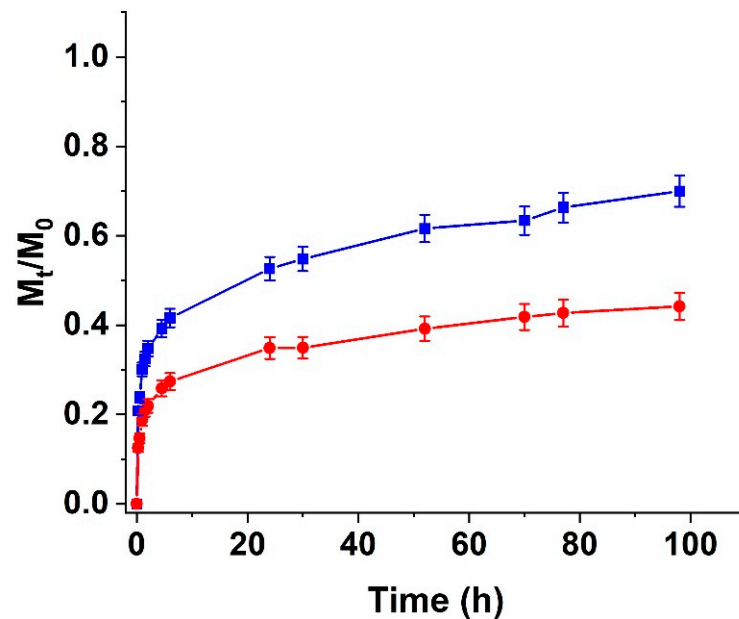


Figure 10. CUR release from H_{ALG} (blue line) and H_{ALG-GO} (red line) as a function of time. The CUR-to-hydrogel ratio (by weight) was 2.5%.

Suitable mathematical models for the determination of the release kinetics helped in understanding the mechanisms of drug release.

In detail, we applied four different models, namely, the zero-order, first-order, Ritger–Peppas, and Peppas–Sahlin equations [69,70].

For the analysis of the kinetic parameters, we applied nonlinear methods to avoid any distortions created in the error distribution by a logarithmic linearization approach.

The first equation applied was the zero-order kinetic model (Equation (3)):

$$\frac{M_t}{M_0} = k_0 t \quad (3)$$

Then, the first-order kinetic model was applied (Equation (4)):

$$\frac{M_t}{M_0} = a(1 - e^{-k_1 t}) \quad (4)$$

Model 3 was described by the Ritger–Peppas Equation (5):

$$\frac{M_t}{M_0} = k_R t^n \quad (5)$$

Model 4 was given by the Peppas–Sahlin Equation (6):

$$\frac{M_t}{M_0} = k'_S t^m + k''_S t^{2m} \quad (6)$$

Here, t is the release time; k_0 , k_1 , k_R , k'_S , and k''_S are the zero-order, first-order, Ritger–Peppas, Fickian diffusion, and anomalous diffusion kinetic constants; a is the first-order release coefficient; n is the Ritger–Peppas coefficient.

In zero-order kinetics that indicate a steady-state concentration profile, the release kinetics are independent of the concentration of the released drug; variation in concentration did not affect the observed drug diffusion, with the release being very slow. On

the contrary, first-order kinetics indicated concentration-dependent processes in which the difference between the drug concentration inside and outside the dosage form acted as the driving force [69]. For swelling-controlled delivery vehicles, the semiempirical “power law” model proposed by Ritger and Peppas can be applied [70]. This model assumed an exponential proportionality between the amount of drug released and time, with the exponent describing the release mechanism driven by a Fickian diffusion ($n \leq 0.50$ for hydrogel films) or anomalous transport processes ($0.50 < n < 1.0$). Finally, the model proposed by Peppas and Sahlin allowed the contributions of Fickian and anomalous phenomena to be quantified over the release rate depending on the prevalence of k'_S (Fickian diffusion) or k''_S (anomalous contributions) [70].

In our conditions, for both H_{ALG} and H_{ALG-GO}, it was clearly evident that the release mechanism was governed by the diffusion of CUR molecules through the swollen hydrogel matrix, since for both zero- and first-order kinetics, R² values lower than 0.85 were recorded (Table 1).

Table 1. Kinetic parameters of CUR release from hybrid and blank ALG hydrogels.

Sample	Zero Order (Equation (3))		First Order (Equation (4))		Ritger–Peppas (Equation (5))			Peppas–Sahlin (Equation (6))				
	R ²	k_1 (10 ^{−3})	R ²	k_2	R ²	k_R	n	R ²	m	k'_S	k''_S (10 ^{−2})	$\frac{k'_S}{k''_S}$
H _{ALG}	0.692	9.36	0.794	0.52	0.996	0.29	0.19	0.998	0.21	0.31	1.7	18
H _{ALG-GO}	0.690	6.02	0.826	0.38	0.993	0.19	0.19	0.997	0.24	0.20	2.0	10

On the contrary, a good fit was obtained between the experimental and theoretical data when Equations (4) and (5) were applied (R² > 0.99 in all cases). Finally, the determination of the k'_S/k''_S ratio allowed for the effect of the incorporation of the GO nanosheet within the polymer network to be highlighted. For both the H_{ALG} and H_{ALG-GO} samples, indeed, the prevalence of k'_S over k''_S was recorded, but the hybrid hydrogel showed a more significant involvement in anomalous phenomena, since the k'_S/k''_S ratio was reduced to almost half when compared to samples that did not contain the carbon nanostructure. This can be attributed to the strong affinity of CUR for GO, which modified the release mechanism due to the involvement of π – π stacking interactions between drug and delivery vehicles, while weak hydrogen bonds were mainly involved in the loading of CUR into H_{ALG}.

4. Conclusions

In this study, we presented experimental evidence that a novel hybrid H_{ALG-GO} hydrogel can be used as a valuable platform for controlling the release of bioactive agents, such as CUR, due to the higher affinity of the GO surface for aromatic species.

As a synthetic strategy, an ionic crosslinking by means of calcium ions was selected to increase the amount of GO being incorporated within the polymer network and to avoid the use of any other chemical species. Suitable physico-chemical characterization allowed the assessment of the homogeneous incorporation of all hydrogel components and the determination of their influence on the morphological, thermal, and water-affinity behaviors of the hybrid system. In detail, GO was found to increase the thermal stability and to reduce the loss of integrity in water media, while CUR was able to enhance the biocompatibility whilst simultaneously acting as a powerful anticancer agent in SCC-25 cancer cells, with the cytotoxic efficiency being strictly related to the CUR-to-hydrogel ratios. The determination of the CUR release profiles, which were extensively investigated through suitable modeling, clearly proved that the presence of GO led to a prolonged CUR release, suggesting the possibility of extending the therapeutic efficiency of the delivery device over time.

Further experiments will be performed to assess the ex vivo and in vivo suitability of the hybrid hydrogels, as well as to determine the most effective CUR loading amount.

Author Contributions: Conceptualization, L.F.M., G.C., O.V., V.V. and S.H.; methodology, G.C., O.V. and V.V.; validation, G.C., O.V. and V.V.; formal analysis, L.F.M. and P.S.; investigation, L.F.M., P.S., M.C. and T.S.-H.; resources, S.H.; data curation, L.F.M. and P.S.; writing—original draft preparation, L.F.M. and G.C.; writing—review and editing, O.V., V.V., M.M. and S.H.; visualization, M.C.; supervision, B.B., M.M. and S.H.; funding acquisition, S.H. All authors have read and agreed to the published version of the manuscript.

Funding: The publication of this article was funded by the Open Access Fund of the Leibniz Association.

Institutional Review Board Statement: Not applicable.

Informed Consent Statement: Not applicable.

Data Availability Statement: Not applicable.

Acknowledgments: The authors wish to thank Marco Naumann for the FTIR data collection, as well as Katrin Wruck and Sandra Schiemenz for their valuable help regarding technical support and laboratory assistance.

Conflicts of Interest: The authors declare no conflict of interest.

References

1. Singh, D.P.; Herrera, C.E.; Singh, B.; Singh, S.; Singh, R.K.; Kumar, R. Graphene oxide: An efficient material and recent approach for biotechnological and biomedical applications. *Mater. Sci. Eng. C-Mater.* **2018**, *86*, 173–197. [[CrossRef](#)] [[PubMed](#)]
2. Ahmed, M.K.; Mansour, S.F.; Al-Wafi, R. Nanofibrous scaffolds of epsilon-polycaprolactone containing Sr/Se-hydroxyapatite/graphene oxide for tissue engineering applications. *Biomed. Mater.* **2021**, *16*, 045030. [[CrossRef](#)] [[PubMed](#)]
3. Gollavelli, G.; Ling, Y.C. Multi-functional graphene as an in vitro and in vivo imaging probe. *Biomaterials* **2012**, *33*, 2532–2545. [[CrossRef](#)] [[PubMed](#)]
4. Zhang, M.F.; Li, Y.; Su, Z.Q.; Wei, G. Recent advances in the synthesis and applications of graphene-polymer nanocomposites. *Polym. Chem.* **2015**, *6*, 6107–6124. [[CrossRef](#)]
5. Panwar, N.; Soehartono, A.M.; Chan, K.K.; Zeng, S.W.; Xu, G.X.; Qu, J.L.; Coquet, P.; Yong, K.T.; Chen, X.Y. Nanocarbons for Biology and Medicine: Sensing, Imaging, and Drug Delivery. *Chem. Rev.* **2019**, *119*, 9559–9656. [[CrossRef](#)]
6. Zhao, X.B.; Wei, Z.H.; Zhao, Z.P.; Miao, Y.L.; Qiu, Y.D.; Yang, W.J.; Jia, X.; Liu, Z.Y.; Hou, H.W. Design and Development of Graphene Oxide Nanoparticle/Chitosan Hybrids Showing pH-Sensitive Surface Charge-Reversible Ability for Efficient Intracellular Doxorubicin Delivery. *ACS Appl. Mater. Interfaces* **2018**, *10*, 6608–6617. [[CrossRef](#)]
7. Liu, W.; Zhang, X.Y.; Zhou, L.; Shang, L.; Su, Z.Q. Reduced graphene oxide (rGO) hybridized hydrogel as a near-infrared (NIR)/pH dual-responsive platform for combined chemo-photothermal therapy. *J. Colloid Interface Sci.* **2019**, *536*, 160–170. [[CrossRef](#)]
8. Zhang, C.; Liu, Z.F.; Zheng, Y.; Geng, Y.D.; Han, C.; Shi, Y.M.; Sun, H.B.; Zhang, C.; Chen, Y.J.; Zhang, L.Y.; et al. Glycyrrhetic Acid Functionalized Graphene Oxide for Mitochondria Targeting and Cancer Treatment In Vivo. *Small* **2018**, *14*, 1703306. [[CrossRef](#)]
9. Javanbakht, S.; Pooresmaeil, M.; Namazi, H. Green one-pot synthesis of carboxymethylcellulose/Zn-based metal-organic framework/graphene oxide bio-nanocomposite as a nanocarrier for drug delivery system. *Carbohydr. Polym.* **2019**, *208*, 294–301. [[CrossRef](#)]
10. Rao, Z.Q.; Ge, H.Y.; Liu, L.L.; Zhu, C.; Min, L.; Liu, M.; Fan, L.H.; Li, D. Carboxymethyl cellulose modified graphene oxide as pH-sensitive drug delivery system. *Int. J. Biol. Macromol.* **2018**, *107*, 1184–1192. [[CrossRef](#)]
11. Chu, J.; Shi, P.P.; Yan, W.X.; Fu, J.P.; Yang, Z.; He, C.M.; Deng, X.Y.; Liu, H.P. PEGylated graphene oxide-mediated quercetin-modified collagen hybrid scaffold for enhancement of MSCs differentiation potential and diabetic wound healing. *Nanoscale* **2018**, *10*, 9547–9560. [[CrossRef](#)] [[PubMed](#)]
12. Wang, C.; Zhang, Z.Q.; Chen, B.B.; Gu, L.Q.; Li, Y.; Yu, S.W. Design and evaluation of galactosylated chitosan/graphene oxide nanoparticles as a drug delivery system. *J. Colloid Interface Sci.* **2018**, *516*, 332–341. [[CrossRef](#)] [[PubMed](#)]
13. Wang, C.M.; Wang, X.Y.; Chen, Y.; Fang, Z. In-vitro photothermal therapy using plant extract polyphenols functionalized graphene sheets for treatment of lung cancer. *J. Photochem. Photobiol. B* **2020**, *204*, 111587. [[CrossRef](#)] [[PubMed](#)]
14. Hatamie, S.; Akhavan, O.; Sadmezhaad, S.K.; Ahadian, M.M.; Shirolkar, M.M.; Wang, H.Q.Q. Curcumin-reduced graphene oxide sheets and their effects on human breast cancer cells. *Mater. Sci. Eng. C-Mater.* **2015**, *55*, 482–489. [[CrossRef](#)]
15. Wang, H.; Liu, Y.; Chen, Z.; Sun, L.; Zhao, Y. Anisotropic structural color particles from colloidal phase separation. *Sci. Adv.* **2020**, *6*, eaay1438. [[CrossRef](#)]
16. Maus, A.; Strait, L.; Zhu, D. Nanoparticles as delivery vehicles for antiviral therapeutic drugs. *Eng. Regen.* **2021**, *2*, 31–46. [[CrossRef](#)]
17. Fiakos, G.; Kuang, Z.; Lo, E. Improved skin regeneration with acellular fish skin grafts. *Eng. Regen.* **2020**, *1*, 95–101. [[CrossRef](#)]
18. Chen, Y.; Lu, Y.; Lee, R.J.; Xiang, G.Y. Nano Encapsulated Curcumin: And Its Potential for Biomedical Applications. *Int. J. Nanomed.* **2020**, *15*, 3099–3120. [[CrossRef](#)]

19. Cirillo, G.; Curcio, M.; Spizzirri, U.G.; Vittorio, O.; Tucci, P.; Picci, N.; Iemma, F.; Hampel, S.; Nicoletta, F.P. Carbon nanotubes hybrid hydrogels for electrically tunable release of Curcumin. *Eur. Polym. J.* **2017**, *90*, 1–12. [[CrossRef](#)]
20. Tomeh, M.A.; Hadianamrei, R.; Zhao, X.B. A Review of Curcumin and Its Derivatives as Anticancer Agents. *Int. J. Mol. Sci.* **2019**, *20*, 1033. [[CrossRef](#)]
21. Ghasemi, F.; Shafiee, M.; Banikazemi, Z.; Pourhanifeh, M.H.; Khanbabaei, H.; Shamshirian, A.; Moghadam, S.A.; ArefNezhad, R.; Sahebkar, A.; Avan, A.; et al. Curcumin inhibits NF- κ B and Wnt/ β -catenin pathways in cervical cancer cells. *Pathol. Res. Pract.* **2019**, *215*, 152556. [[CrossRef](#)] [[PubMed](#)]
22. Kotha, R.R.; Luthria, D.L. Curcumin: Biological, Pharmaceutical, Nutraceutical, and Analytical Aspects. *Molecules* **2019**, *24*, 2930. [[CrossRef](#)]
23. Srivastava, N.S.; Srivastava, R.A.K. Curcumin and quercetin synergistically inhibit cancer cell proliferation in multiple cancer cells and modulate Wnt/ β -catenin signaling and apoptotic pathways in A375 cells. *Phytomedicine* **2019**, *52*, 117–128. [[CrossRef](#)] [[PubMed](#)]
24. Bevacqua, E.; Curcio, M.; Saletta, F.; Vittorio, O.; Cirillo, G.; Tucci, P. Dextran-Curcumin Nanosystems Inhibit Cell Growth and Migration Regulating the Epithelial to Mesenchymal Transition in Prostate Cancer Cells. *Int. J. Mol. Sci.* **2021**, *22*, 7013. [[CrossRef](#)] [[PubMed](#)]
25. Vollono, L.; Falconi, M.; Gaziano, R.; Iacovelli, F.; Dika, E.; Terracciano, C.; Bianchi, L.; Campione, E. Potential of Curcumin in Skin Disorders. *Nutrients* **2019**, *11*, 2169. [[CrossRef](#)]
26. di Luca, M.; Curcio, M.; Valli, E.; Cirillo, G.; Voli, F.; Butini, M.E.; Farfalla, A.; Pantuso, E.; Leggio, A.; Nicoletta, F.P.; et al. Combining antioxidant hydrogels with self-assembled microparticles for multifunctional wound dressings. *J. Mater. Chem. B* **2019**, *7*, 4361–4370. [[CrossRef](#)]
27. LoTempio, M.M.; Veena, M.S.; Steele, H.L.; Ramamurthy, B.; Ramalingam, T.S.; Cohen, A.N.; Chakrabarti, R.; Srivatsan, E.S.; Wang, M.B. Curcumin suppresses growth of head and neck squamous cell carcinoma. *Clin. Cancer Res.* **2005**, *11*, 6994–7002. [[CrossRef](#)]
28. Wang, D.; Veena, M.S.; Stevenson, K.; Tang, C.; Ho, B.; Suh, J.D.; Duarte, V.M.; Faull, K.F.; Mehta, K.; Srivatsan, E.S.; et al. Liposome-Encapsulated Curcumin Suppresses Growth of Head and Neck Squamous Cell Carcinoma In vitro and in Xenografts through the Inhibition of Nuclear Factor kappa B by an AKT-Independent Pathway. *Clin. Cancer Res.* **2008**, *14*, 6228–6236. [[CrossRef](#)]
29. Khaffif, A.; Schantz, S.P.; Chou, T.C.; Edelstein, D.; Sacks, P.G. Quantitation of chemopreventive synergism between (-)-epigallocatechin-3-gallate and curcumin in normal, premalignant and malignant human oral epithelial cells. *Carcinogenesis* **1998**, *19*, 419–424. [[CrossRef](#)]
30. Phillips, J.M.; Clark, C.; Herman-Ferdinandez, L.; Moore-Medlin, T.; Rong, X.H.; Gill, J.R.; Clifford, J.L.; Abreo, F.; Nathan, C.A.O. Curcumin Inhibits Skin Squamous Cell Carcinoma Tumor Growth In Vivo. *Otolaryngol.-Head Neck Surg.* **2011**, *145*, 58–63. [[CrossRef](#)]
31. Rosner, M. Squamous Cell Carcinoma. In *Essentials of Ophthalmic Oncology*; Slack Incorporated: West Deptford, NJ, USA, 2009; pp. 35–36.
32. Sarogni, P.; Mapanao, A.K.; Marchetti, S.; Kusmic, C.; Voliani, V. A Standard Protocol for the Production and Bioevaluation of Ethical In Vivo Models of HPV-Negative Head and Neck Squamous Cell Carcinoma. *ACS Pharmacol. Transl. Sci.* **2021**, *4*, 1227–1234. [[CrossRef](#)] [[PubMed](#)]
33. Santi, M.; Mapanao, A.K.; Cappello, V.; Voliani, V. Production of 3D Tumor Models of Head and Neck Squamous Cell Carcinomas for Nanotheranostics Assessment. *ACS Biomater. Sci. Eng.* **2020**, *6*, 4862–4869. [[CrossRef](#)] [[PubMed](#)]
34. Santi, M.; Mapanao, A.K.; Biancalana, L.; Marchetti, F.; Voliani, V. Ruthenium arene complexes in the treatment of 3D models of head and neck squamous cell carcinomas. *Eur. J. Med. Chem.* **2021**, *212*, 113143. [[CrossRef](#)] [[PubMed](#)]
35. Mapanao, A.K.; Santi, M.; Voliani, V. Combined chemo-photothermal treatment of three-dimensional head and neck squamous cell carcinomas by gold nano-architectures. *J. Colloid Interface Sci.* **2021**, *582*, 1003–1011. [[CrossRef](#)]
36. Santi, M.; Mapanao, A.K.; Cassano, D.; Vlamidis, Y.; Cappello, V.; Voliani, V. Endogenously-Activated Ultrasmall-in-Nano Therapeutics: Assessment on 3D Head and Neck Squamous Cell Carcinomas. *Cancers* **2020**, *12*, 1063. [[CrossRef](#)]
37. Hassanzadeh, K.; Buccarello, L.; Dragotto, J.; Mohammadi, A.; Corbo, M.; Feligioni, M. Obstacles against the Marketing of Curcumin as a Drug. *Int. J. Mol. Sci.* **2020**, *21*, 6619. [[CrossRef](#)]
38. Gupta, S.C.; Patchva, S.; Aggarwal, B.B. Therapeutic Roles of Curcumin: Lessons Learned from Clinical Trials. *AAPS J.* **2013**, *15*, 195–218. [[CrossRef](#)]
39. Burgos-Moron, E.; Calderon-Montano, J.M.; Salvador, J.; Robles, A.; Lopez-Lazaro, M. The dark side of curcumin. *Int. J. Cancer* **2010**, *126*, 1771–1775. [[CrossRef](#)]
40. Yang, X.X.; Li, C.M.; Li, Y.F.; Wang, J.; Huang, C.Z. Synergistic antiviral effect of curcumin functionalized graphene oxide against respiratory syncytial virus infection. *Nanoscale* **2017**, *9*, 16086–16092. [[CrossRef](#)]
41. Liang, Y.P.; Zhao, X.; Hu, T.L.; Chen, B.J.; Yin, Z.H.; Ma, P.X.; Guo, B.L. Adhesive Hemostatic Conducting Injectable Composite Hydrogels with Sustained Drug Release and Photothermal Antibacterial Activity to Promote Full-Thickness Skin Regeneration During Wound Healing. *Small* **2019**, *15*, 1900046. [[CrossRef](#)]
42. Rehman, S.R.U.; Augustine, R.; Zahid, A.A.; Ahmed, R.; Tariq, M.; Hasan, A. Reduced Graphene Oxide Incorporated GelMA Hydrogel Promotes Angiogenesis For Wound Healing Applications. *Int. J. Nanomed.* **2019**, *14*, 9603–9617. [[CrossRef](#)] [[PubMed](#)]

43. Wang, J.; Liu, C.H.; Shuai, Y.; Cui, X.Y.; Nie, L. Controlled release of anticancer drug using graphene oxide as a drug-binding effector in konjac glucomannan/sodium alginate hydrogels. *Colloids Surf. B* **2014**, *113*, 223–229. [[CrossRef](#)] [[PubMed](#)]
44. Kolanthai, E.; Sindu, P.A.; Khajuria, D.K.; Veerla, S.C.; Kuppaswamy, D.; Catalani, L.H.; Mahapatra, D.R. Graphene Oxide-A Tool for the Preparation of Chemically Crosslinking Free Alginate-Chitosan-Collagen Scaffolds for Bone Tissue Engineering. *ACS Appl. Mater. Interfaces* **2018**, *10*, 12441–12452. [[CrossRef](#)]
45. Chen, K.H.; Ling, Y.Z.; Cao, C.; Li, X.Y.; Chen, X.; Wang, X.Y. Chitosan derivatives/reduced graphene oxide/alginate beads for small-molecule drug delivery. *Mater. Sci. Eng. C-Mater.* **2016**, *69*, 1222–1228. [[CrossRef](#)] [[PubMed](#)]
46. Choe, G.; Oh, S.; Seok, J.M.; Park, S.A.; Lee, J.Y. Graphene oxide/alginate composites as novel bioinks for three-dimensional mesenchymal stem cell printing and bone regeneration applications. *Nanoscale* **2019**, *11*, 23275–23285. [[CrossRef](#)] [[PubMed](#)]
47. Sudhakar, K.; Moloi, S.J.; Rao, K.M. Graphene oxide/poly(N-isopropyl acrylamide)/sodium alginate-based dual responsive composite beads for controlled release characteristics of chemotherapeutic agent. *Iran. Polym. J.* **2017**, *26*, 521–530. [[CrossRef](#)]
48. Strober, W. Trypan Blue Exclusion Test of Cell Viability. *Curr. Protoc. Immunol.* **1997**, *21*, A.3B.1–A.3B.2. [[CrossRef](#)]
49. Rebers, L.; Reichsollner, R.; Regett, S.; Tovar, G.E.M.; Borchers, K.; Baudis, S.; Southan, A. Differentiation of physical and chemical cross-linking in gelatin methacryloyl hydrogels. *Sci. Rep.* **2021**, *11*, 3256. [[CrossRef](#)]
50. Bialik-Was, K.; Krolicka, E.; Malina, D. Impact of the Type of Crosslinking Agents on the Properties of Modified Sodium Alginate/Poly(vinyl Alcohol) Hydrogels. *Molecules* **2021**, *26*, 2381. [[CrossRef](#)]
51. di Luca, M.; Vittorio, O.; Cirillo, G.; Curcio, M.; Czuban, M.; Voli, F.; Farfalla, A.; Hampel, S.; Nicoletta, F.P.; Iemma, F. Electro-responsive graphene oxide hydrogels for skin bandages: The outcome of gelatin and trypsin immobilization. *Int. J. Pharm.* **2018**, *546*, 50–60. [[CrossRef](#)]
52. Marrella, A.; Lagazzo, A.; Barberis, F.; Catelani, T.; Quarto, R.; Scaglione, S. Enhanced mechanical performances and bioactivity of cell laden-graphene oxide/alginate hydrogels open new scenario for articular tissue engineering applications. *Carbon* **2017**, *115*, 608–616. [[CrossRef](#)]
53. Bajas, D.; Vlase, G.; Mateescu, M.; Grad, O.A.; Bunoiu, M.; Vlase, T.; Avram, C. Formulation and Characterization of Alginate-Based Membranes for the Potential Transdermal Delivery of Methotrexate. *Polymers* **2021**, *13*, 161. [[CrossRef](#)] [[PubMed](#)]
54. Khalili, D. Graphene oxide: A promising carbocatalyst for the regioselective thiocyanation of aromatic amines, phenols, anisols and enolizable ketones by hydrogen peroxide/KSCN in water. *New J. Chem.* **2016**, *40*, 2547–2553. [[CrossRef](#)]
55. Badria, F.A.; Abdelaziz, A.E.; Hassan, A.H.; Elgazar, A.A.; Mazyed, E.A. Development of Provesicular Nanodelivery System of Curcumin as a Safe and Effective Antiviral Agent: Statistical Optimization, In Vitro Characterization, and Antiviral Effectiveness. *Molecules* **2020**, *25*, 5668. [[CrossRef](#)]
56. Farivar, F.; Yap, P.L.; Karunakaran, R.U.; Losic, D. Thermogravimetric Analysis (TGA) of Graphene Materials: Effect of Particle Size of Graphene, Graphene Oxide and Graphite on Thermal Parameters. *C-J. Carbon Res.* **2021**, *7*, 41. [[CrossRef](#)]
57. Zheng, H.C.; Yang, J.S.; Han, S.Y. The synthesis and characteristics of sodium alginate/graphene oxide composite films crosslinked with multivalent cations. *J. Appl. Polym. Sci.* **2016**, *133*, 43616. [[CrossRef](#)]
58. Bajpai, S.K.; Sharma, S. Investigation of swelling/degradation behaviour of alginate beads crosslinked with Ca²⁺ and Ba²⁺ ions. *React. Funct. Polym.* **2004**, *59*, 129–140. [[CrossRef](#)]
59. Khavari, A.; Nyden, M.; Weitz, D.A.; Ehrlicher, A.J. Composite alginate gels for tunable cellular microenvironment mechanics. *Sci. Rep.* **2016**, *6*, 30854. [[CrossRef](#)]
60. Joddar, B.; Garcia, E.; Casas, A.; Stewart, C.M. Development of functionalized multi-walled carbon-nanotube-based alginate hydrogels for enabling biomimetic technologies. *Sci. Rep.* **2016**, *6*, 32456. [[CrossRef](#)]
61. Cirillo, G.; Pantuso, E.; Curcio, M.; Vittorio, O.; Leggio, A.; Iemma, F.; De Filipo, G.; Nicoletta, F.P. Alginate Bioconjugate and Graphene Oxide in Multifunctional Hydrogels for Versatile Biomedical Applications. *Molecules* **2021**, *26*, 1355. [[CrossRef](#)]
62. Chang, Y.L.; Yang, S.T.; Liu, J.H.; Dong, E.; Wang, Y.W.; Cao, A.N.; Liu, Y.F.; Wang, H.F. In vitro toxicity evaluation of graphene oxide on A549 cells. *Toxicol. Lett.* **2011**, *200*, 201–210. [[CrossRef](#)] [[PubMed](#)]
63. Qiu, Y.; Wang, Z.Y.; Owens, A.C.E.; Kulaots, I.; Chen, Y.T.; Kane, A.B.; Hurt, R.H. Antioxidant chemistry of graphene-based materials and its role in oxidation protection technology. *Nanoscale* **2014**, *6*, 11744–11755. [[CrossRef](#)] [[PubMed](#)]
64. Qin, W.; Li, X.; Bian, W.W.; Fan, X.J.; Qi, J.Y. Density functional theory calculations and molecular dynamics simulations of the adsorption of biomolecules on graphene surfaces. *Biomaterials* **2010**, *31*, 1007–1016. [[CrossRef](#)] [[PubMed](#)]
65. Zhang, J.; Cao, H.Y.; Wang, J.Q.; Wu, G.D.; Wang, L. Graphene Oxide and Reduced Graphene Oxide Exhibit Cardiotoxicity Through the Regulation of Lipid Peroxidation, Oxidative Stress, and Mitochondrial Dysfunction. *Front. Cell Dev. Biol.* **2021**, *9*, 616888. [[CrossRef](#)] [[PubMed](#)]
66. Bonner, M.Y.; Arbiser, J.L. The antioxidant paradox: What are antioxidants and how should they be used in a therapeutic context for cancer. *Future Med. Chem.* **2014**, *6*, 1413–1422. [[CrossRef](#)] [[PubMed](#)]
67. Halliwell, B. The antioxidant paradox. *Lancet* **2000**, *355*, 1179–1180. [[CrossRef](#)]
68. Jorgenson, T.C.; Zhong, W.X.; Oberley, T.D. Redox Imbalance and Biochemical Changes in Cancer. *Cancer Res.* **2013**, *73*, 6118–6123. [[CrossRef](#)]
69. Malekjani, N.; Jafari, S.M. Modeling the release of food bioactive ingredients from carriers/nanocarriers by the empirical, semiempirical, and mechanistic models. *Compr. Rev. Food Sci. Food Saf.* **2021**, *20*, 3–47. [[CrossRef](#)]
70. Unagolla, J.M.; Jayasuriya, A.C. Drug transport mechanisms and in vitro release kinetics of vancomycin encapsulated chitosan-alginate polyelectrolyte microparticles as a controlled drug delivery system. *Eur. J. Pharm. Sci.* **2018**, *114*, 199–209. [[CrossRef](#)]